Journal of Materials Chemistry A

Accepted Manuscript

ROYAL SOCIETY OF CHEMISTRY

www.rsc.org/materialsA

J. Mater. Chem. A

ARTICLE

Stannous ions reducing graphene oxide at room temperature to produce SnOx-porous carbon nanofiber flexible mats as binder-free anodes for lithium-ion batteries

Received 00th January 20xx,
Accepted 00th January 20xx

DOI: 10.1039/x0xx00000x

www.rsc.org/

Feilong Yan,[a] Xuan Tang [a], Yuehua Wei [a], Libao Chen[b], Guozhong Cao*[c,d], Ming Zhang*[a], Taihong Wang [a]

Tin oxides with high theoretical capacities as anodes for lithium-ion batteries always suffer from the electrically disconnect issue of active materials owing to huge volume changes. In this work, the flexible mats composed of ultra-small SnO_x nanoparticles, graphene, and carbon fibers are synthesized by reducing graphene oxide with stannous ions at room temperature and following treatments. SnO_x nanoparticles, including SnO and SnO_2, with ultra-small diameters of approximate 4 nm are embedding in the matrix composed of carbon fiber and graphene to form composite fibers which are woven into flexible mats without any binders. As binder-free anodes for lithium-ion batteries, SnO_x-graphene-carbon fiber mats can deliver a high reversible capacity of 545 mA h g^{-1} after 1000 cycles at a current density of 200 mA g^{-1}, which is much better than those of SnO_x-carbon fiber mats. The improvement of SnO_x-graphene-carbon fiber mats can be attributed to the ultra-small size of SnO_x nanoparticles and the double-protection arising from both graphene and carbon fibers.

1 Introduction

Great attention has been devoted to lithium-ion batteries (LIBs) with high energy density and long cycle stability to meet the increasing demand in many fields,[1] such as portable electronics,[2] electric vehicles,[2-6] as well as large-scale stationary energy storage systems.[4, 7] Nevertheless, the energy density, power density, and cyclic stability of commercial LIBs whose theoretical capacities are just 137 and 372 mA h g^{-1} for $LiCoO_2$ (50% delithiation) and graphite need to be further improved.[1] Tin oxides/Tin as anodes for LIBs have attracted considerable attention owing to their high theoretical specific capacities,[8] such as SnO_2 (781 mA h g^{-1}),[9-11] SnO (875 mA h g^{-1})[12] and Sn (992 mA h g^{-1}),[1, 5, 13-15] whose theoretical capacities are 2.5 times higher than that of commercial graphite (372 mA h g^{-1}).[13, 16]

However, tin oxides suffer from significant capacity fading due to enormous volume changes during lithiation/delithiation process.[5, 10, 17] Several approaches have been developed to address this issue. For example, tin oxides were nanosized to minimize the strain during volume changes.[4, 17-19] This strategy, however, would result in a relatively high irreversible capacity in the initial cycle, arising from the formation of enlarged solid electrolyte interface (SEI) films because of the high specific area of nanomatierials.[20] Another approach is to integrate tin oxides with carbonaceous materials to accommodate their huge volume changes, including amorphous carbon, mesoporous carbon, graphene, carbon nanotubes (CNTs) or carbon nanofiber mats.[4, 5] For example, SnO_2/graphene composites have been synthesized using tin salts and graphene oxide (GO) as raw materials by many methods,[11] such as $NaBH_4$ reduction,[21] hydrothermal growth,[22] and in situ deposition.[5] Commonly, additional reductants are used in above routes to reduce GO. Although GO have been demonstrated to be reduced by stannous ions at a relatively high temperature without any reductants in recently papers,[23, 24] the reduction of GO by stannous ion at room temperature with little energy consumption has not been reported. In addition, GO remains highly resistive even after reduction, which is not optimal for energy storage applications. GO also can control metal oxides' morphology and size.[25]

To realize the high power density and good cyclic stability of tin oxides based on composites as anodes for LIBs, they should possess two important features: high electrical conductance and fast diffusion channels for Li^+.[5, 26, 27] Tin oxides/graphene composites usually have relatively high conductance because of the present of graphene.[26, 28] However, diffusion of Li^+ may be blocked by either the binder

[a] Key Laboratory for Micro-Nano Optoelectronic Devices of Ministry of Education, School of Physics and Microelectronics, State Key Laboratory for Chemo/Biosensing and Chemometrics, Hunan University,Changsha, 410082, P.R. China; E-mail: zhangming@hnu.edu.cn.
[b] State Key Laboratory for Power Metallurgy, Central South University, Changsha, 10083, P.R. China.
[c] Department of Materials Science & Engineering, University of Washington, Seattle, Washington, 98195, USA.
[d] Beijing Institute of Nanoenergy and Nanosystems, Chinese Academy of Sciences, Beijing 100083, China; E-mail: gzcao@uw.edu.
[e] Electronic Supplementary Information (ESI) available: SEM images of different sample, FT-IR spectra for rGO and GO and TEM images of the SGCF-700. See DOI: 10.1039/x0xx00000x

(like PVDF, polyvinylidene difluoride) or the stacking of graphene sheets in tin oxides/grapheme composites.[10, 29] This issue could be partially solved by introducing some carbon nanoparticles between graphene sheets to enlarge the interspace.[30] The Li^+ diffusion blocked by binders cannot be easily improved unless preparing binder-free electrodes,[29, 31] such as growth nanomaterials on nickel foams. Nevertheless, the micrometer-sized nickel foam with relatively low specific surface area cannot load nanomaterials at sufficiently high content of active materials. Therefore, it is of great significance to support tin oxides to fabricate binder-free anodes for LIBs.[29, 31]

Although modifying them with either carbon fibers or graphene is a useful strategy to maintain their structure stability and improve the electrochemical properties, the double-protection strategy of tin oxides by both carbon fibers and graphene have not been reported. In this study, flexible hierarchical mats of SnO_x-graphene-carbon nanofibers (SGCFs) were synthesized by reducing GO with stannous ions at room temperature, and followed electrospinning and thermal treatment. The ultra-small tin oxides with diameters of approximate 4 nm were anchored on carbon fibers by chemical bonds. Even though the content of graphene and SnO_x in the nanofibers was very low, the flexible mats exhibited a high specific capacity at a large current density, and excellent cyclic stability as binder-free anodes for LIBs. Such superior electrochemical results were ascribed to carbon and graphene double protection strategy and the ultra-small size of tin oxides.

2 Experimental details

2.1 Materials synthesis

Polyacrylonitrile (PAN, Mw = 150 000, Sigma-Aldrich Co., Ltd., USA), Tin(II) chloride dihydrate ($SnCl_2{\cdot}2H_2O$, Alfa Aesar Co., Ltd., USA), and N,N- dimethylformamide (DMF, J. T. Baker Co., Ltd., USA) were used without any further purication.

Graphene oxide (GO) was prepared according to our group previous literature.[29] GO was dispersed in DMF at a concentration of about 0.4 mg mL^{-1}, and the suspension was processed with ultrasonic waves for 30 min. To prepare the precursor solution for electrospinning, 0.43g PAN were dissolved in GO-DMF solution and vigorously stirred for 3 h at 30℃ temperature, forming the brown solution; 1.5 mmol $SnCl_2{\cdot}2H_2O$ were dissolved in DMF and vigorously stirred for 1 h at room temperature, forming the transparent solution in Figure 1a. After this, the vigorous solution was added in the brown solution with dropper drop by drop. To prepare comparative carbon fibers, a precursor without GO was also prepared. A precursor for nanofibers without graphene was prepared by a similar way without GO. All of the precursor solution was transferred into a 5mL syringe with a stainless steel needle (with an inner diameter of 0.71 mm). A syringe pump controlled the flow rate of the precursor solution to about 0.2 mL h^{-1}. A piece of aluminum foil used as the collector was vertically positioned about 15 cm away from the needle. The needle was connected to a high voltage DC power supply to obtain a voltage of 11-14 kV. Under these conditions, PAN-$SnCl_2{\cdot}2H_2O$ and PAN-GO-$SnCl_2{\cdot}2H_2O$ nanofibers were generated and formed mats. After pre-oxidized at 230 ℃ in air for 6 h, the resulting brown films (PAN-GO-$SnCl_2{\cdot}2H_2O$) were treated at 600 ℃ and 700 ℃ in argon for 2 h in order to carbonize the PAN and decompose $SnCl_2{\cdot}2H_2O$, and the product is denoted as SGCF-600 and SGCF-700, respectively. The SnO_x-C nanofibers (SCFs) were treated in a similar way at 700℃ in order to obtain the corresponding samples, and the product is denoted as SCF-700.

2.2 Material characterization

The morphologies of the samples were studied by a field emission gun scanning electron microscope (Hitachi S-4800, 5 kV). Transmission electron microscopy (TEM) and high-resolution TEM (HRTEM) investigations were carried out by a JEOL JEM-2100F microscope. The samples were also analyzed using X-ray photoelectron spectroscopy (XPS, Surface Science Instruments S-probe spectrometer). Elemental analysis of the samples was achieved using energy dispersive spectroscopy (EDS). The thermal gravimetric analysis was performed on a Thermo-Gravimetric Analysis (TGA, PerkinElmer, Diamond TG/DTA) in air with a heating rate of 3.5℃ min^{-1}. The samples were heated from room temperature to 800℃.

2.3 Electrochemical measurements

The mats (including the SGCF-600, and SGCF-700, SCF-700) were directly used as binder-free anodes for electrochemical measurements towards the storage of Li^+. A Celgard 2400 micro porous polypropylene membrane was used as a separator to assemble coin cells (CR 2025). The electrolyte used was a solution of 1 M $LiPF_6$ in ethylene carbonate–dimethyl carbonate (1:1 by volume). Pieces of pure lithium foil were used as both counters and reference electrodes. All of the cells were assembled in an argon-filled glove-box with the moisture and the oxygen levels less than 1 ppm. Discharge and charge measurements were carried out using an Arbin BT2000 and a LAND battery testing system with the cut off potentials being 0.005 V for discharge and 3 V for charge. The cyclic voltammetry results were collected on an electrochemical workstation (CHI660B).

3 Results and discussion

3.1 Synthesis mechanism of SnO_x-graphene

A new strategy for preparing graphene by reducing GO with stannous ions was explored for the synthesis of SnO_x-G nanocomposite. As shown in Figure 1a, a light yellow DMF solution containing GO and polya crylonitrile (PAN) were prepared (left) and $SnCl_2{\cdot}H_2O$ was dissolution in DMF to form a colorless solution (right). A brownish mixture, which was the typical color of GO, was achieved by mixing above two solutions,[23, 24] as shown in Figure 1b. The light brown color can be attributed to the dilution of colorless $SnCl_2{\cdot}H_2O$ solution. Then the mixed solution was stirred at room temperature. After stirring for 1 h, the solution (Figure 1c) became darkened as compared to the freshly mixed solution. When stirring for

10 h, the solution turned from brown to black, which was a typical color of graphene (Figure 1e). In this solution, stannous ions have stronger reduction power than components, such as DMF, PAN, H_2O, and Cl^-.[23, 32] The solution color transferring from light brown to dark black is an indication that GO was reduced by stannous ions at room temperature.[23] The scheme in Figure 1f presents the chemical reaction process of stannous ion reducing GO at room temperature and the formation of SnO_2-graphene (SnO_2-G) composites. A possible reaction mechanism of the reduction process is shown in Equation 1 and 2. Firstly, the standard electrode potential in acid of Sn^{4+}/Sn^{2+} ($\varphi_A^{\ominus} = 0.15V$) is much lower than that of Ag^+/Ag ($\varphi_A^{\ominus} = 1.98V$), showing a relative strong reducibility. In addition, the standard electrode potential of Sn^{4+}/Sn^{2+} shows a lower value comparing with that value in acid in base ($\varphi_B^{\ominus} = -0.93V$), indicating a strong reducibility. Previous reported also have demonstrated that stannous ions can reduce Ag^+ to silver metal.[33, 34] Secondly, owing to the strong reducibility of Sn^{2+}, GO could be reduced to graphene and SnO_2 nanoparticles were fixed on the graphene sheets. The organic solvent may be a special factor to improve the reducibility of Sn^{2+} at room temperature as compared with previous studies about the reducibility of $SnCl_2{\cdot}2H_2O$ in a water solution.[23, 32] Furthermore, the intensity of the C=O stretching peak at 1730 cm^{-1} in the FT-IR spectrum of rGO was diminished after reduction (Fig. S2). A weak signal for the C-OH stretching vibration at 3420 cm^{-1} could be ascribed to the vibrations of the adsorbed water molecules. So it could be concluded that GO was reduced by the stannous ions.[23] In addition, the diameters of resulted SnO2 nanoparticles may be decreased by the oxygen-containing groups and the nonaqueous reaction system.[35]

$$Sn^{2+} + 2H_2O \Leftrightarrow Sn(OH)_2 + 2H^+ \quad (1)$$

$$Sn(OH)_2 + GO \rightarrow SnO_2 + G + 2H^+ \quad (2)$$

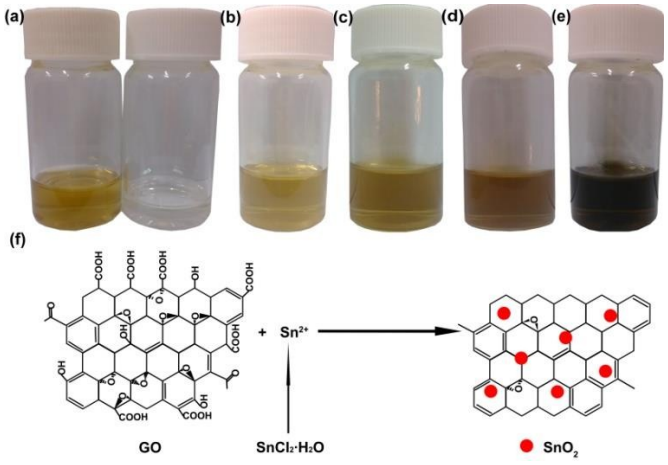

Figure 1 Digital photographs of (a) PAN-GO-DMF solution (left) and $SnCl_2$-DMF solution (right), (b) just mixed solution of PAN, GO, $SnCl_2{\cdot}2H_2O$, and DMF, (c-e) mixed solution after magnetic stirring for 1 h (c), 2 h (d), and one night (e). The time-dependent colors of the mixtures are the evidences of Sn^{2+} reducing GO at room temperature. (f) Illustrates of synthesis procedure of SnO_2-G composites.

3.2 Synthesis and characterization of SGCF flexible mats

After the electrospinning of precursor solution containing PAN and SnO_2-G, the as prepared fibers (PAN-SnO_2-G) were pre-oxidized in air followed by treated at a high temperature in Ar. The electrospun fibers with large length to diameter ratios are easily woven into mats without any binders.[29, 31] The resulted flexible mats were hammered into circular films with diameters of 13 mm, as shown in Figure 2a and Figure 2d. As-prepared PAN-SnO_2-G fibers without any obvious nanoparticles are shown in Figure S1a, indicating the ultra-small diameters of SnO_2. Figure 2b and 2e display the digital photos of the pre-oxidized samples treated at 230 ℃ in air for 6 h. In spite of their diameters decreased to 12 mm and the color changed from white to brown, the circular films were without any obvious variation of shape and thickness. The corresponding SEM image shown in Figure S1b confirms the stability of fibers. After thermal treatment at 700 ℃ in Ar for 2 h, the final black SGCF mats (Figure 2c and 2d) without any cracks are of diameters of about 8 mm, showing good structure stability and flexibility of the mats built by SGCFs. Figure 2g is a typical low magnification SEM image of the continuous SGCF-700 nanofibers, which shows a regular diameter in the range of 120-160 nm and length for several micrometers. In addition, the nanofibers weave into a multilayer and hierarchical network without any binders. An amplified SEM image of SGCF-700 is displayed in Figure 2h, revealing that the surface of SGCF-700 nanofibers is smooth and uniform. Graphene is not directly observed in the SEM image, because graphene with an approximate concentration of 1.2wt% (based on a carbonization yield of 45wt% for PAN) is embedded in the carbon matrix pyrolysised from PAN. As a comparison experiment, no GO was added and the final samples treated at 700 ℃ were SnO_x-C nanofibers which were marked as SCF-700 and shown in Figure 2i (Figure S1 (c)). The diameter of SCF-700 is little smaller than that of SGCF-700, and some cracked fibers are found although the fibers also built a binder-free network. The flexibility of SGCF-700 mats was tested by bending experiments, as shown in Figure 2j, 2k, and 2l. The SGCF-700 mat with a 180 degree bending was not broken (Figure 2j). The degree of bending can decrease as the improvement of tweezers interspace (Figure 2k). After the bending experiments, the mat without any cracks is of an integral structure, confirming the excellent flexibility of SGCF-700 mats.

The detailed morphological and structural features of the SGCFs were also characterized by TEM. Figure 3a shows a typical TEM image of SGCF-700. No aggregated SnO_x nanoparticles are found on the smooth surface of the fibers, indicating that the particles were embedded in SGCFs. This phenomenon can be confirmed by more TEM images (Figure S3) at different magnifications. The fracture of SGCFs could be ascribed to the ultrasonication during preparing samples for TEM test. The high magnification TEM image is shown in Figure 3b. The lighter color in the fibers represents the carbon matrix and the darker color represents SnO_x. This image reveals that

the ultra-small nanoparticles with diameters of approximate 4 nm (black dots) were well dispersed in SGCFs, suggesting good compatibility between carbon and the nanoparticles. The size of SnO_x is very close to the perfect diameter of SnO_2 nanoparticles as anodes for LIBs reported by a previous paper.[36] To further explore the structure of the composites, high-resolution TEM (HRTEM) studies were carried out, as presented in Figure 3c and 3d. An ultra-small SnO_x was embedded in the SGCFs. Two planes with d-spacing of 0.275 nm in Figure 3c and 0.26 nm in Figure 3d were observed on the surface of SGCFs. Those values are highly consistent with the (011) planes of SnO and the (002) planes of SnO_2,[5, 37] indicating the presence of ultra-small SnO_x nanoparticles in SGCFs and the transformation of SnO_2 to SnO during the treatment at 700 ℃. The ultra-small size of SnO_x nanoparticles could be attributed to the inhibition of carbon matrix and graphene on the growth of nanoparticles.[35] The presence and distribution of Sn elements were further verified by TEM element mapping (Figure S4a–d). Figure S4c confirmed the homogenous distribution of Sn on CNFs. Other elements, such as C, N, and O, also were uniformly distributed on CNFs. Taking into account of the TEM results, it can be concluded that ultrafine SnO_x nanoparticles are homogenously distributed on CNFs.

The chemical composition at the surface of SGCF-700 may be investigated by X-ray photoelectron spectroscopy (XPS). As shown in Figure 4a, the Sn $3d_{5/2}$ peak can be deconvoluted to two peaks. The peaks at 486.7 and 487.4 eV are ascribed to Sn^{2+} and Sn^{4+}, corresponding to atom ratios of 61.3% and 38.7% respectively.[1, 5] This result is consistent with the conclusion of

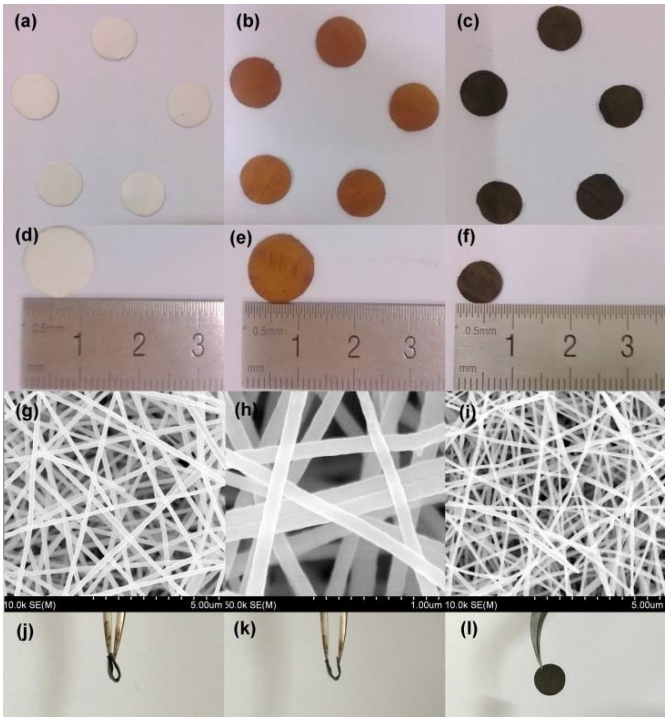

Figure 2 Digital photographs of as-prepared mats (a, d), the mat treated at 230℃ (b, e), and SGCF-700 mats(c, f). Those images show the size shrinkage of the mats. Low (g) and high-magnification (h) SEM images of the SGCF-700 mat; (i) SEM image of SCF-700 mats. (j), (k) and (l) are the digital photographs of SGCF-700, which show the flexibility of SGCF-700 mats.

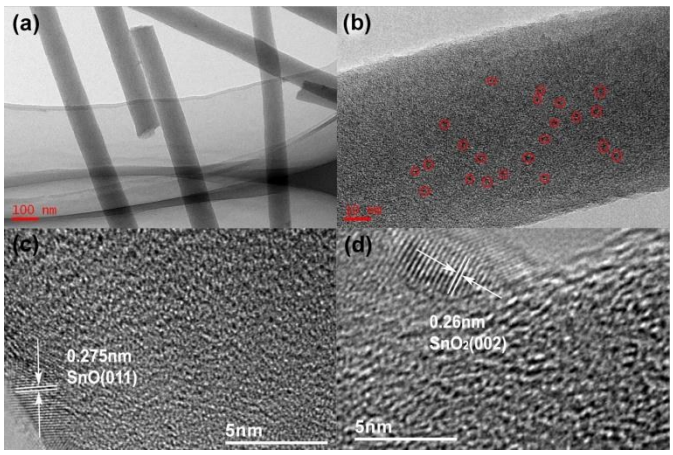

Figure 3 (a) and (b) display the low and high magnification TEM images of the SGCF-700. The ultra-small particles in (b) are marked as cycles. (c), (d) show HRTEM images of the nanoparticles indicated by circles in (b), conforming the existence of both SnO and SnO_2.

TEM that there are two tin-based compounds in the SGCF-700. The O 1s spectrum is shown in Figure 4b, which could be deconvoluted to four peaks. The peaks at 531.3, and 533.2 eV are assigned to oxygen in O_2 and H_2O, respectively, which should be attributed to the adsorbed H_2O and O_2 on the carbon matrix/graphite.[1] Another peak at 533.6 eV originated from C-O bonding indicates that the oxygen also bond with carbon. Other peaks at 531.3 and 533.2 eV can be indexed to oxygen and water.[1] The remaining peak may be an evidence of Sn-O bonding (532.4 eV), which was directly explained that the ultra-small tin oxides with diameters of 4 nm were anchored on carbon fibers by chemical bonds.[1] The full XPS spectrum of SGCF-700 in Figure 4c demonstrated that there was nitrogen and carbon in SGCFs except tin and oxygen. The fine XPS spectrum of N 1s shows tow peaks at about 398.4 and 400.8 eV, which could be indexed to pyridine-type and conjugated nitrogen. Both of the above nitrogen types have positive effects on the storage of lithium ions, especially pyridine-type nitrogen.[29] Besides, nitrogen doping could improve the conductivity of carbon, and result in enhanced the properties of lithium ion storage.[1, 4] The EDS spectrum in Figure 4d shows the presence of carbon, oxygen, tin, and nitrogen in SGCFs, which is consistent with the results of XPS results in Figure 4c. The copper can be assigned to the sample holder for TEM characterization. Thus, SnO_x nanoparticles (including SnO_2 and SnO) were chemically embedded in nitrogen doped carbon fibers.

Thermogravimetric analysis (TGA) was carried out to gain insight into the chemical composition of SGCF-700 in air, and the corresponding result is shown in Figure 5. From the TGA curve, SGCF-700 has 68.22% weight loss from 300 to 633℃ that can be assigned to combustion of graphene and carbon in air forming CO_2.[4] This carbon weight loss agrees well with the result from XPS analysis. The final product of TGA is SnO_2 with weight of 33.8%. Considering the transformation of SnO to SnO_2 with weight increase of 11.9% and Sn^{2+} with an atom ratio of 61.3%, the weight ratio can be estimated to be 18.5wt%

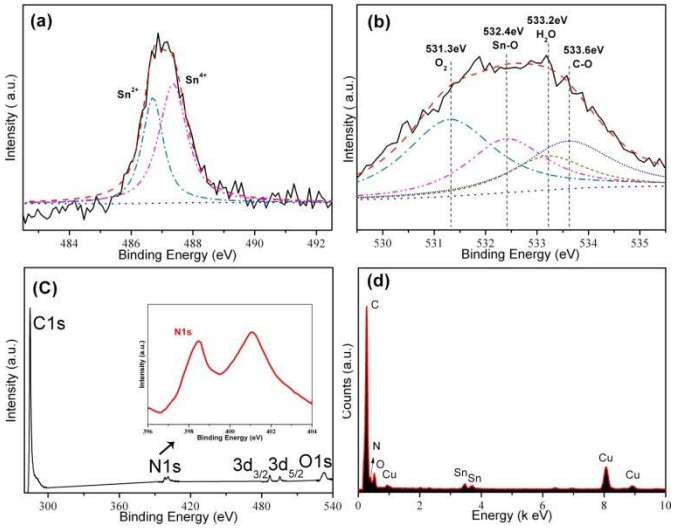

Figure 4 (a) Sn 3d XPS spectra of SGCF-700 mats; (b) High resolution O1s XPS spectrum of SGCF-700; (c) The full XPS spectrum of SGCF-700 (Insert shows the N 1s spectrum of SGCF-700); (d) EDS of SGCF-700 mats collected on TEM.

for SnO, 13.1wt% for SnO_2, 67.3wt for carbon fibers, and o.1wt% for graphene. The detail approach for calculation is shown in Supporting Information.

Nitrogen adsorption studies were carried out in order to investigate the surface area and pore volume of as-prepared porous SGCF-700 mats (Figure S5). BET results show that porous SGCF-700 nanofibers have a surface area of about 14.9 $m^2\ g^{-1}$. In addition, porous SGCF-700 nanofibers also have a pore volume of about 0.208 $cm^3\ g^{-1}$. Figure S5b demonstrates that most of the pores are smaller than 50 nm in diameter, and SGCF-700 mats are mainly composed of mesopores (1–50nm). The BET results demonstrate the formation of porous structure in SGCF-700 mat.

The CV tests were performed to investigate the mechanism of electrochemical reactions, as shown in Figure 6. The cathodic peak of SGCF-700 at about 0.57 V in the first cycle (Figure 6a) is ascribed to the formation of a SEI film and the lithiation of SnO_2 (Equation. 3) which disappears in the following cycles. Another peak in the range of 0 to 0.3 V can be indexed to the intercalation of lithium ions into carbon (Equation. 5) and formation of Li-Sn alloys (Equation. 4).[38-40]

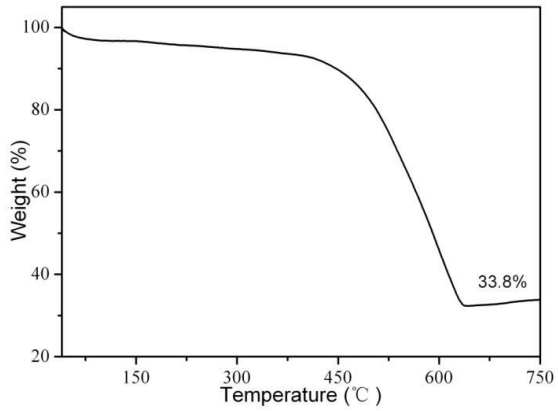

Figure 5 Thermogravimetric analysis (TGA) of the SGCF-700 at a heating rate of 3.5 ℃ /min in air with a flow rate of 20 mL/min.

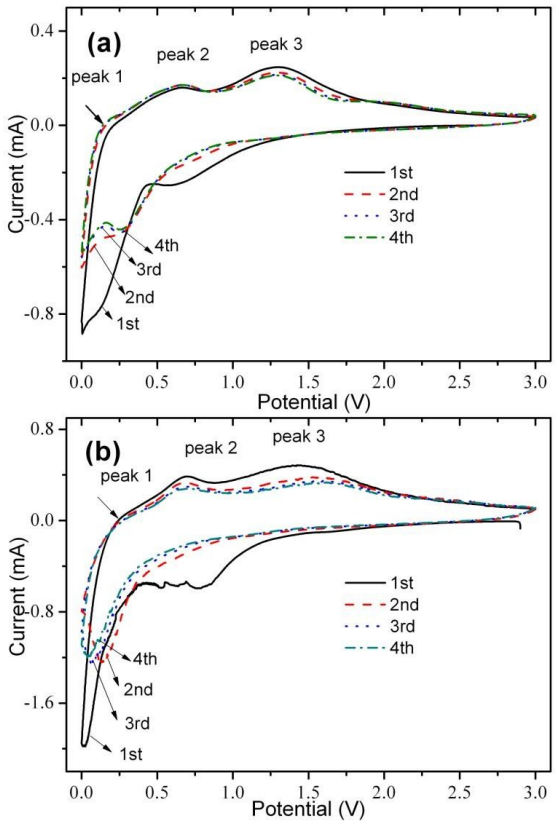

Figure 6 CV curves of (a) SGCF-700 and (b) SCF-700 mats at a scan rate of 0.3 mV s^{-1}.

During the anodic scan, three peaks are found. The peak at about 0.1 V could be attributed to the delithiation of graphite carbon. Another anodic peak at 0.65 V can be ascribed to the delithiation of Li-Sn alloys (Equation. 4). The anodic peak at about 1.35 V may be deconvoluted to two aspects. The first one is the reversible transfer of Sn^0 to SnO_2, which have been observed in some SnO_2-carbon/graphene composites for LIB.[23, 41, 42] Another possible reaction representing this peak is the reversible lithium ions extracting from the defective sites or micropores of carbon matrix.[43] Further investigation needs to be carried out to make the detail mechanism of this peak clear. Although the CV curves of SCF-700 are similar to those of SGCF-700, there are some differences between them. Firstly, the changes of anodic peaks of SGCF-700 at 0.65 and 1.35 V are smaller than those of SCF-700 in the initial four cycles, showing an improved cyclic stability of SGCF-700 by introducing graphene although both of them show good cyclic stability from the second to the fourth cycle. Secondly, the peak current ratios of the peak 3 to the peak 2 of SGCF-700 are higher than those of SCF-700, indicating a possible improved reversibility of the reversible transfer of Sn^0 to SnO_2 and lithium ions extracting from the defective sites or micropores of carbon matrix.[44]

$$SnO_x + 2xLi^+ + 2xe^- \rightarrow Sn + xLi_2O \quad (3)$$

$$Sn + xLi^+ + xe^- \Leftrightarrow Li_xSn (0 \le x \le 4.4) \quad (4)$$

$$6C + yLi^+ + ye^- \Leftrightarrow Li_yC_6 (0 \le y \le 1) \quad (5)$$

The charge-discharge curves of SGCF-700 mats are shown in Figure 7a. It is worth noting that the poorly defined plateau at about 0.8 V associated with the reduction of SnO_2 to Sn becomes indiscernible in the following cycles, which suggests the irreversibility of this reaction within the narrow voltage window.[45] The potential profiles of SGCF-700 electrodes at a current density of 200 mA g^{-1} presented excellent discharge and charge capacities of 1272.6 and 828.7 mA h g^{-1} in the first cycle, corresponding to a Coulombic efficiency (CE) of 65.1%. With increasing the number of cycles, the discharge capacity gradually decayed to 891.6, 639.8, 601.6 and 598 mA h g^{-1} in the 2nd, 100th, 200th and 400th cycles, respectively. The large capacity loss (34.9%) in the first cycle is generally attributed to the irreversible formation of the SEI film during the first discharge process.

Figure 7b displays the cyclic properties of SGCF-700 mats in the potential range of 0.005 to 3.0 V at a current density of 200 mA g^{-1}. The CE of the second cycle exceeds 92.3%. The high CE indicates that the embedment of SnO_x nanoparticles in

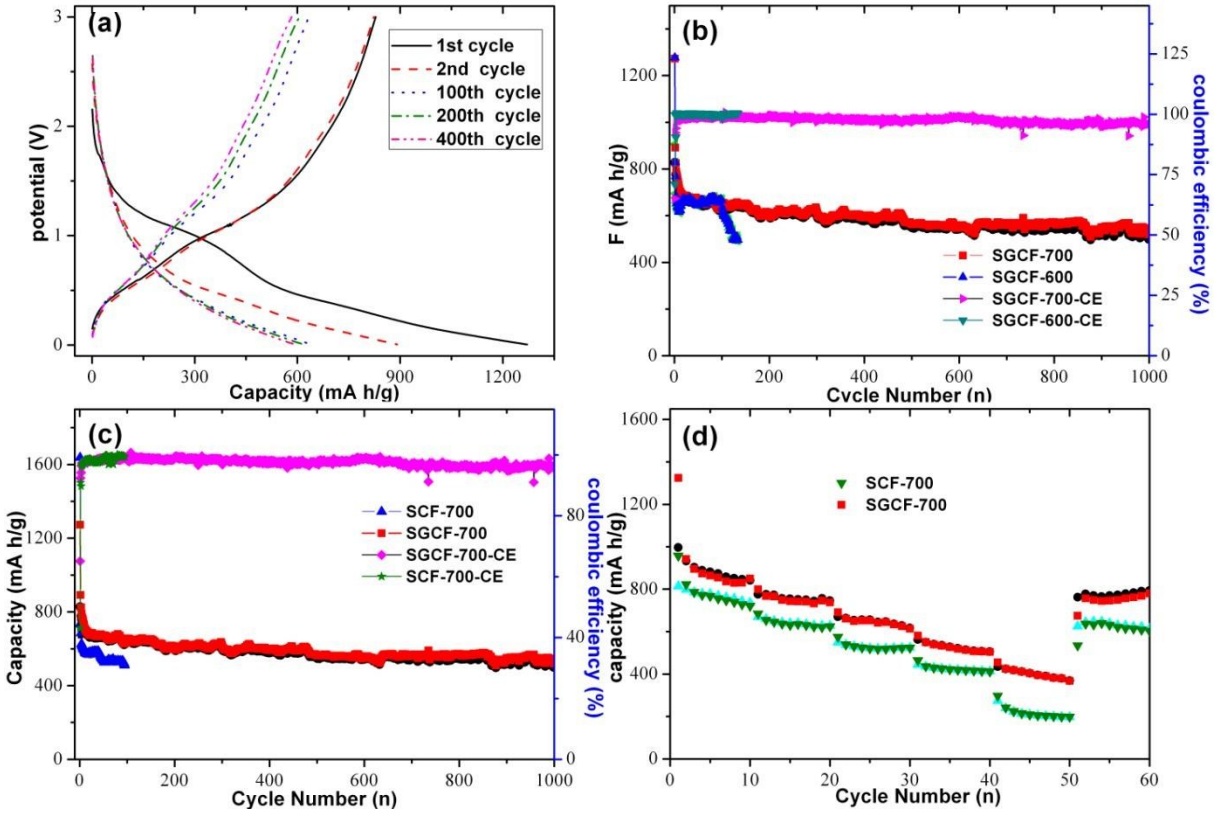

Figure 7 (a) Charge-discharge voltage profiles of SGCF-700 mats at the 1st, 2nd, 100th, 200th, 400th cycles at a current density of 200 mA g^{-1}; (b) and (c) show cyclic properties of SGCF-700 mats in comparison with SGCF-600 and SCF-700 at current densities of 200 mA g^{-1}; (d) Rate capability of SGCF-700 as compare with SCF-700 at current densities of 100, 200, 500, 1000, 2000, and 100 mA g^{-1}, respectively. All of specific capacities in this study were calculated based on the weight of whole mats.

the carbon matrix can largely avoid detrimental reactions between SnO_x and electrolyte, which is in good agreement with the CV result. The high capacity should benefit from the ultra-small particles of SnO_x nanoparticles and porous carbon network structure, which enables the full utilization of SnO_x nanoparticles. More importantly, after several cycles the reversible capacity is stabled at 100%. The slow shrinkage of charge/discharge curves after the first cycle implies the high cycling stability of the as-prepared composite. The reasons for this enhancement are caused by the synergistic effect of electrospinning and optimal heat treatment. For comparison, SGCF-600 composite anode delivered an initial discharge capacity of 1277 mA h g^{-1} with a CE of 70.9%. The properties of SGCF-700 are just a little better than those of SGCF-600. But after 135 cycles, SGCF-600 anodes only delivered a capacity of 496 mA h g^{-1}, which are much lower than SGCF-700 anodes. The inferior properties of SGCF-600 could be attributed to the low degree of carbonization and poor conductance of the nanofibers. This result agrees with a recent study on PAN-based carbon for LIBs.[29] In detail, the porous carbon nanofiber mats prepared by electrospinning act as a buffering matrix can prevent the agglomeration of SnO_2 particles, volume expansion and mechanical stress during Li alloying and dealloying.[31] The porous carbon nanofiber is used an electrical conductor to compensate for the drawback of semiconductor such as SnO_2 and Li_2O. And it helps promote the decomposition of SnO_x as a semiconductor into Sn and Li_2O. Besides, the porous carbon nanofibers allow the charge transfer and mass transfer to facilitate lithiation/delithiation due to high electronic conductivity.[5, 29]

Figure 7c compares the cyclic stability and specific capacities of SGCF-700 and SCF-700 mats. It is clearly that SGCF-700 mats exhibit much better cycling stability than that

of SCF-700 electrodes. SCF-700 mats delivered an initial discharge capacity of 1637 mA h g^{-1} with a CE of 43.0%. Although the initial discharge of SGCF-700, which is 1273 mA h g^{-1}, is lower than that of SCF-700. SGCF-700 could deliver a discharge capacity of 640 mA h g^{-1} in the 100th cycle, 1.25 times that of SCF-700 in the same cycle. Even after 480 cycles, SGCF-700 mats still delivered a discharge capacity of 600 mA h g^{-1}, which is almost 50% higher than that of traditional graphitic anode (372 mA h g^{-1}). Besides, the CE of SGCF-700 also was higher than that of SCF-700 in the fourth cycle in spite of their CE are almost 100% in the following cycles. Besides, the high CE in SGCF-700 anodes after four cycles suggests high reversibility of SGCF-700 mats for the storage of lithium ions. Considering the difference between SGCF-700 and SCF-700, the improved properties of SGCF-700 could be attributed to presence of graphene, which can affect the growth of nanoparticles resulting in ultra-small nanoparticles and suppress the agglomeration of tin alloys.[10, 28] Another reason for the high properties of SGCF-700 may be the ultra-small diameter (4 nm) of SnO_x nanoparticles which is close to the optimizing size (about 3-4 nm) of SnO_2 for Li^+ storage.[36]

Table 1 Comparison of capacities for various SnO_x-carbon electrodes

Material	Capacity (mA h g^{-1})	Current density	Ref.
SnO_x-CNF	674, 100th cycle	500 mA g^{-1}	5
SnO_x-CNF	510, 40th cycle	30 mA g^{-1}	14
SnO_x-CNF	450, 30th cycle	25 mA g^{-1}	46
SnO_x-CNF	649, 100th cycle	30 mA g^{-1}	47
SnO_x-CNF	608, 200th cycle	500 mA g^{-1}	48
SnO_x-CNF	520, 100th cycle	200 mA g^{-1}	49
SnO_x-CNF	512, 200th cycle	200 mA g^{-1}	50
SnO_x-G-CNF	600, 480th cycle	200 mA g^{-1}	This
SnO_x-G-CNF	545, 1000th cycle	200 mA g^{-1}	study

Figure 7d shows the rate capacities of SGCF-700 and SCF-700. SGCF-700 maintains reversible capacities of 850,737, 613, 504, and 368 mA h g^{-1} at current densities of 100, 200, 500, 1000, and 2000 mA g^{-1}, respectively. These values are higher than those of SCF-700 at the corresponding current densities. This improvement could be attributed to the enhanced conductance arising from graphene. The synergistic effects arising from the ultra-small SnO_x particles within the porous carbon nanofibers and graphene are further expounded for comparison. It is proved that the graphene can be used to improve the mechanical properties of porous carbon nanofiber mats made by electrospinning.

To demonstrate the superior electrochemical performance of SnO_x-carbon nanofiber (CNF) freestanding electrodes developed in this study, Table 1 compares the capacities and cycles of the electrodes prepared using similar SnO_x-based materials and approaches taken from recent reports. Indeed, the SnO_x-graphene-carbon fiber composites obtained in this study presents a relatively high capacities and best cyclic stability.

In order to investigate the lithium-driven structural and morphological changes during the charge and discharge processes, we performed ex-situ SEM analysis on the SGCF-700 electrodes before cycling and after the 1000th cycle and SCF-700 electrodes after the 100th cycle at a current density of 200 mA g^{-1}, and the SEM images are shown in Figure 8. It can be found from Figure 8 that the structure and morphology of SGCF-700 electrodes maintain integrity (Figure 8a and Figure S5a). However, SCF-700 electrodes can be found that the much aggregate was on the porous carbon nanofibers surfaces (Figure 8b), and protuberant particles with diameters of 1-4 um were dispersed in SGCFs (Figure S5b). The stark contrast between the two samples demonstrates that the graphene not only can obviously improve specific capacity, but also can keep the cycling stability for LIBs.

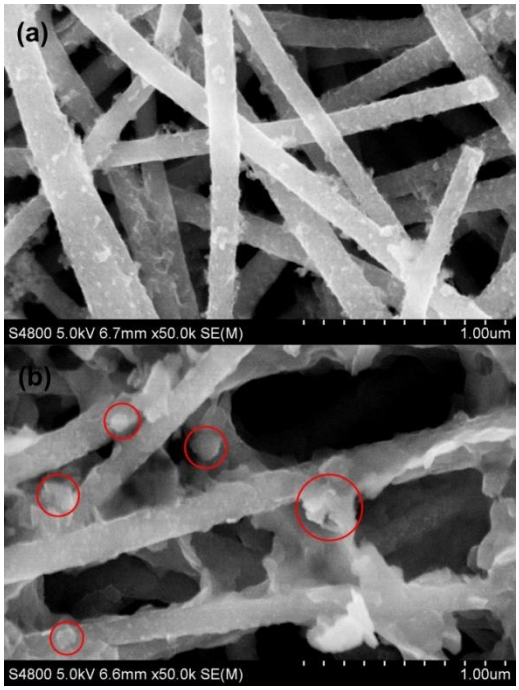

Figure 8 (a) SEM image of SGCF-700 after 1000 cycles, (b) SEM image of SCF-700 after 100 cycles. Both SGCF-700 and SCF-700 were tested at a current density of 200 mA g^{-1}.

4 Conclusions

Flexible hierarchical porous mats of SGCFs were synthesized by reducing GO with stannous ions at room temperature and following electrospinning route. The SnO_x nanoparticles (including SnO and SnO_2) with ultra-small sizes were chemically embedded in the graphene-carbon nanofiber mats. As binder-free anodes for LIBs, the flexible SGCF mats obtained at 700 ℃ can deliver a discharge capacity of 545 after 1000 cycles at a current density of 200 mA g^{-1} while it is only 509 mA h g^{-1} for the mats without graphene in the 100th cycle. The rate capacities of SGCF mats are also higher than those of SCFs as the same current densities. The excellent properties of SGCF mats can be ascribed to the hierarchical networks severed as the highway for electrons and diffusion channels for ions, and graphene to maintain the structural stability of SnO_x nanoparticles and improve the conductivity of CNFs. It is believed that this strategy may be used for the synthesis of the composites based on other compounds of

valence variable element, graphene, and carbon fibers for the storage and transformation of energy.

Acknowledgements

This research work has been financially supported by National Natural Science Foundation of China (51404103, 61376073, 21373081), the Hunan Provincial Natural Science Foundation of China (11JJ7004, 14JJ3067), and Fundamental Research Funds for the Central Universities.

Notes and references

1 Z. Zhu, S. Wang, J. Du, Q. Jin, T. Zhang, F. Cheng and J. Chen, *Nano Letters*, 2013, **14**, 153-157.
2 X. Zhou, L.-J. Wan and Y.-G. Guo, *Advanced Materials*, 2013, **25**, 2152-2157.
3 Y. Yu, L. Gu, C. Zhu, P. A. van Aken and J. Maier, *Journal of the American Chemical Society*, 2009, **131**, 15984-15985.
4 G. Zhang, J. Zhu, W. Zeng, S. Hou, F. Gong, F. Li, C. C. Li and H. Duan, *Nano Energy*, 2014, **9**, 61-70.
5 B. Zhang, Y. Yu, Z. Huang, Y.-B. He, D. Jang, W.-S. Yoon, Y.-W. Mai, F. Kang and J.-K. Kim, *Energy & Environmental Science*, 2012, **5**, 9895-9902.
6 G. Wang, H. Liu, J. Liu, S. Qiao, G. M. Lu, P. Munroe and H. Ahn, *Advanced Materials*, 2010, **22**, 4944-4948.
7 M. Zhang, Y. Li, E. Uchaker, S. Candelaria, L. Shen, T. Wang and G. Cao, *Nano Energy*, 2013, **2**, 769-778.
8 Y. N. Ko, S. B. Park and Y. C. Kang, *Small*, 2014, **10**, 3240-3245.
9 P. Meduri, C. Pendyala, V. Kumar, G. U. Sumanasekera and M. K. Sunkara, *Nano Letters*, 2009, **9**, 612-616.
10 S.-M. Paek, E. Yoo and I. Honma, *Nano Letters*, 2008, **9**, 72-75.
11 X. Zhou, Y.-X. Yin, L.-J. Wan and Y.-G. Guo, *Journal of Materials Chemistry*, 2012, **22**, 17456-17459.
12 K. Sakaushi, Y. Oaki, H. Uchiyama, E. Hosono, H. Zhou and H. Imai, *Small*, 2010, **6**, 776-781.
13 J. Zhu, J. Jiang, Y. Feng, G. Meng, H. Ding and X. Huang, *ACS Applied Materials & Interfaces*, 2013, **5**, 2634-2640.
14 L. Zou, L. Gan, R. Lv, M. Wang, Z.-h. Huang, F. Kang and W. Shen, *Carbon*, 2011, **49**, 89-95.
15 K. T. Lee, Y. S. Jung and S. M. Oh, *Journal of the American Chemical Society*, 2003, **125**, 5652-5653.
16 N. Yesibolati, M. Shahid, W. Chen, M. N. Hedhili, M. C. Reuter, F. M. Ross and H. N. Alshareef, *Small*, 2014, **10**, 2849-2858.
17 H.-X. Zhang, C. Feng, Y.-C. Zhai, K.-L. Jiang, Q.-Q. Li and S.-S. Fan, *Advanced Materials*, 2009, **21**, 2299-2304.
18 Y. Yu, L. Gu, C. Wang, A. Dhanabalan, P. A. van Aken and J. Maier, *Angewandte Chemie International Edition*, 2009, **48**, 6485-6489.
19 19.X. W. Lou, C. M. Li and L. A. Archer, *Advanced Materials*, 2009, **21**, 2536-2539.
20 E. Peled, C. Menachem, D. Bar‐Tow and A. Melman, *Journal of The Electrochemical Society*, 1996, **143**, L4-L7.
21 X.-L. Wang, M. Feygenson, M. C. Aronson and W.-Q. Han, *The Journal of Physical Chemistry C*, 2010, **114**, 14697-14703.
22 J. Lin, Z. Peng, C. Xiang, G. Ruan, Z. Yan, D. Natelson and J. M. Tour, *ACS Nano*, 2013, **7**, 6001-6006.
23 M. Zhang, D. Lei, Z. Du, X. Yin, L. Chen, Q. Li, Y. Wang and T. Wang, *Journal of Materials Chemistry*, 2011, **21**, 1673-1676.
24 M. Zhang, D. Lei, X. Yu, L. Chen, Q. Li, Y. Wang, T. Wang and G. Cao, *Journal of Materials Chemistry*, 2012, **22**, 23091-23097.
25 H. Wang, H. S. Casalongue, Y. Liang and H. Dai, *Journal of the American Chemical Society*, 2010, **132**, 7472-7477.
26 26.Y. Wang, H. C. Zeng and J. Y. Lee, *Advanced Materials*, 2006, **18**, 645-649.
27 L. Qie, W.-M. Chen, Z.-H. Wang, Q.-G. Shao, X. Li, L.-X. Yuan, X.-L. Hu, W.-X. Zhang and Y.-H. Huang, *Advanced Materials*, 2012, **24**, 2047-2050.
28 X. Zhou, J. Bao, Z. Dai and Y.-G. Guo, *The Journal of Physical Chemistry C*, 2013, **117**, 25367-25373.
29 M. Zhang, F. Yan, X. Tang, Q. Li, T. Wang and G. Cao, *Journal of Materials Chemistry A*, 2014, **2**, 5890-5897.
30 E. Yoo, J. Kim, E. Hosono, H.-s. Zhou, T. Kudo and I. Honma, *Nano Letters*, 2008, **8**, 2277-2282.
31 M. Zhang, E. Uchaker, S. Hu, Q. Zhang, T. Wang, G. Cao and J. Li, *Nanoscale*, 2013, **5**, 12342-12349.
32 B. Zhao, G. Zhang, J. Song, Y. Jiang, H. Zhuang, P. Liu and T. Fang, *Electrochimica Acta*, 2011, **56**, 7340-7346.
33 Y. Kobayashi, V. Salgueiriño-Maceira and L. M. Liz-Marzán, *Chemistry of Materials*, 2001, **13**, 1630-1633.
34 Z. Zhang, C. Shao, Y. Sun, J. Mu, M. Zhang, P. Zhang, Z. Guo, P. Liang, C. Wang and Y. Liu, *Journal of Materials Chemistry*, 2012, **22**, 1387-1395.
35 H. Wang, J. T. Robinson, G. Diankov and H. Dai, *Journal of the American Chemical Society*, 2010, **132**, 3270-3271.
36 C. Kim, M. Noh, M. Choi, J. Cho and B. Park, *Chemistry of Materials*, 2005, **17**, 3297-3301.
37 J. Zhu, D. Lei, G. Zhang, Q. Li, B. Lu and T. Wang, *Nanoscale*, 2013, **5**, 5499-5505.
38 M.-S. Park, G.-X. Wang, Y.-M. Kang, D. Wexler, S.-X. Dou and H.-K. Liu, *Angewandte Chemie*, 2007, **119**, 764-767.
39 C. Guan, X. Wang, Q. Zhang, Z. Fan, H. Zhang and H. J. Fan, *Nano Letters*, 2014, **14**, 4852-4858.
40 J. Zhu, G. Zhang, X. Yu, Q. Li, B. Lu and Z. Xu, *Nano Energy*, 2014, **3**, 80-87.
41 X. Wang, X. Zhou, K. Yao, J. Zhang and Z. Liu, *Carbon*, 2011, **49**, 133-139.
42 Y. Chen, Q. Z. Huang, J. Wang, Q. Wang and J. M. Xue, *Journal of Materials Chemistry*, 2011, **21**, 17448-17453.
43 B. Guo, X. Wang, P. F. Fulvio, M. Chi, S. M. Mahurin, X.-G. Sun and S. Dai, *Advanced Materials*, 2011, **23**, 4661-4666.
44 C.-M. Wang, W. Xu, J. Liu, J.-G. Zhang, L. V. Saraf, B. W. Arey, D. Choi, Z.-G. Yang, J. Xiao, S. Thevuthasan and D. R. Baer, *Nano Letters*, 2011, **11**, 1874-1880.
45 L. Zhang, H. B. Wu, B. Liu and X. W. Lou, *Energy & Environmental Science*, 2014, **7**, 1013-1017.
46 Y. Yu, Q. Yang, D. Teng, X. Yang and S. Ryu, *Electrochemistry Communications*, 2010, **12**, 1187-1190.
47 H.-R. Jung and W.-J. Lee, *Journal of Electroanalytical Chemistry*, 2011, **662**, 334-342.
48 X. Zhou, Z. Dai, S. Liu, J. Bao and Y.-G. Guo, *Advanced Materials*, 2014, **26**, 3943-3949.
49 M. Zou, J. Li, W. Wen, Y. Lin, H. Lai and Z. Huang, *Materials Research Bulletin*, 2014, **60**, 868-871.
50 S. Li, H. Yue, Q. Wang, W. Xie and D. He, *Materials Letters*, 2014, **116**, 271-274.

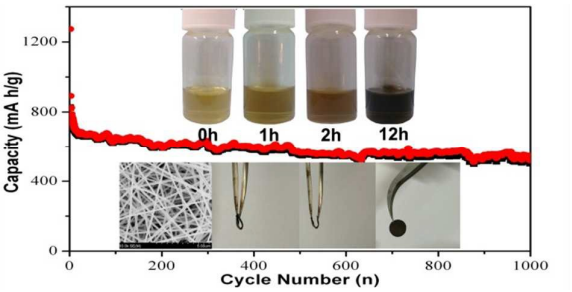

SnO_x-porous carbon nanofiber flexible mats deliver a high reversible capacity of 545 mA h g^{-1} after 1000 cycles at 200 mA g^{-1}.